Optical Properties of Se_2^- and Se_2 Color Centers in the Red Selenium Ultramarine with the Sodalite Structure

H. Schlaich,[†] G.-G. Lindner,[‡] J. Feldmann,[†] E. O. Göbel,[†] and D. Reinen*[,‡]

Fachbereich Physik and Fachbereich Chemie, Zentrum für Materialforschung der Philipps-Universität Marburg, D-35032 Marburg, Germany

Received February 24, 1999

The unique optical properties of Se_2^- radicals located in the cages of the sodalite structure are reported. By means of luminescence, photoluminescence excitation, and absorption spectroscopy, three different centers are identified. Two of them are Se_2^- anions in sites with presumably a tetrahedral Na_4^{4+} coordination and a Na_3^{3+} environment with cation deficiency, respectively, giving rise to a red luminescence band with two different progressions. The third center is the intermediate Se_2 molecule, created photochemically by UV laser excitation. It induces an additional blue luminescence. The electronic properties of the Se_2^- centers, particularly in the excited states, are significantly influenced by steric constraints imposed by the limited space in the sodalite host polyhedra. Thus, the sodalite structure can be viewed as a model system for studying effects of this kind on chromophores imbedded in the cages of the zeolite-type lattice.

1. Introduction

In this paper we study the optical properties of Se_2^- color centers in the cages of the sodalite lattice. The first to prepare red compounds of this type were Plique and Guimet about a century ago.[1,2] The synthesis of the selenium ultramarine follows the one of the blue sulfur ultramarine by replacing S by Se.[3−5] UV/vis and Raman spectroscopy as well as powder X-ray diffraction analysis revealed a zeolite-like sodalite structure for the selenium compound as well and made most probable that the Se_2^- radical anion is the color center.[4−6] To definitely identify and characterize the chromophore, single crystals of the red ultramarine are necessary, however.

We recently succeeded in growing transparent weakly red selenium-doped sodalite crystals for the first time.[4,5] They emit a broad and efficient luminescence in the visible and near-IR regions, which is ascribed to Se_2^-, observed only in alkali metal halides so far. The properties of Se_2^- in the latter host compounds were extensively studied and are well understood.[7−13] Te_2^- chromophores can be incorporated into the sodalite cages as well, leading to green and blue ultramarine-type single crystals.[14] By studying the electronic and vibrational properties of the red ultramarine, we find that the Se_2^- entities are rather weakly bonded to the sodalite frame, steric constraints in the sodalite cages playing an important role. This may be of interest in connection with the creation of semiconductor quantum dots in zeolite cages, where research is in progress.[15]

Two remarkable differences between the optical spectra of the Se_2^- chromophores in the sodalite matrix and in the alkaline metal halides, respectively, exist. While in the former host two luminescence bands are observed, in the latter case that in the blue region is lacking. Further the optical spectra of the selenium ultramarines do not depend on the preparation method—in contrast to those of the Se_2^--doped alkaline halides—which makes their quantitative interpretation rather difficult.[11,16]

The spectroscopic and color properties of chalcogen diradicals, such as X_2 and X_2^- (X = S, Se, Te), in ultramarine-type solids have been reviewed elsewhere.[17] The sodalite lattice can be viewed as an appropriate model host structure for studying the influence of steric constraints on the electronic properties of embedded molecules or anions.

2. Experimental Section

The preparation of the single crystal and powder materials, used for the measurements, is described in detail elsewhere.[4,5] The largest crystal species had a diameter of about 0.5 mm.

The high-resolution photoluminescence (PL) spectra were measured with a 1 m monochromator. In the visible spectral range we used a GaAs photomultiplier (PM) for detection. In the near infrared spectral region a liquid nitrogen cooled Ge PM was employed, with a resolution better than 0.05 nm (<3 cm^{-1}). The 364 nm (27 472 cm^{-1}), 457 nm (21 881 cm^{-1}), and 514 nm (19 455 cm^{-1}) lines of an Ar^+ laser were used for exciting the luminescence. The samples were mounted in a flowing helium cryostat (T < 10 K). For the measurements of the photoluminescence excitation (PLE) spectra the samples were excited with an Ar^+-pumped dye laser, whose wavelength was changed by a

* To whom correspondence should be addressed. Fax: 06421-2828917.
[†] Fachbereich Physik.
[‡] Fachbereich Chemie.

(1) Plique, J. *Bl. Soc. Chim., Paris N.S.* **1877**, *28*, 522.
(2) Guimet, E. *Bl. Soc. Chim., Paris N.S.* **1878**, *29*, 104.
(3) Guimet, J. *Bull. de l'encouragment poer l'industrie nationale*; 1828. See also refs 1 and 2.
(4) Lindner, G.-G.; Reinen, D. *Z. Anorg. Allg. Chem.* **1994**, *620*, 1321 and references therein.
(5) Lindner, G.-G. Farbe, Elektronenstruktur und Konstitution ultramarinartiger Zeolite mit eingelagerten Chalkogenspezies. *Berichte aus der Chemie*; Thesis, Marburg; Verlag Shaker: Aachen, 1994.
(6) Cark, R.; Dines, T.; Kurmoo, M. *Inorg. Chem.* **1983**, *22*, 2767.
(7) Rolfe, J. *J. Chem. Phys.* **1968**, *49*, 4193.
(8) Ikezawa, M.; Rolfe, J. *J. Chem. Phys.* **1973**, *58*, 2024.
(9) Rebane, L.; Khaldre, T. *JETP Lett.* **1977**, *26*, 525.
(10) Vella, G. J.; Rolfe, J. *J. Chem. Phys.* **1974**, *61*, 41.
(11) Murata, H.; Kishigami; T.; Kato, R. *J. Phys. Soc. Jpn.* **1990**, *59*, 506.
(12) Fabian, H.; Fischer, F. *J. Lumin.* **1989**, *43*, 103.
(13) Freiberg, A.; Rebane, L. In *Zero-Phonon Lines and Spectral Hole Burning in Spectroscopy and Photochemistry*; Sild, O., Haller, K., Eds.; Springer: Berlin, Heidelberg, New York, 1988; p 55.
(14) Lindner, G.-G.; Witke, K.; Schlaich, H.; Reinen, D. *Inorg. Chim. Acta* **1996**, *252*, 39.
(15) e.g. Herron, N.; Wang, Y.; Eddy, M. M.; Stucky, G. D.; Cox, D. E.; Moller, K.; Bein, Th. *J. Am. Chem. Soc.* **1989**, *111*, 35.
(16) Cook, J.; Dryden, J.; Ferguson, J. *J. Lumin.* **1986**, *36*, 1.
(17) Reinen, D.; Lindner, G.-G. *Chem. Soc. Rev.* **1999**, *28*, 75.

10.1021/ic990223u CCC: $19.00
Published on Web 06/02/2000

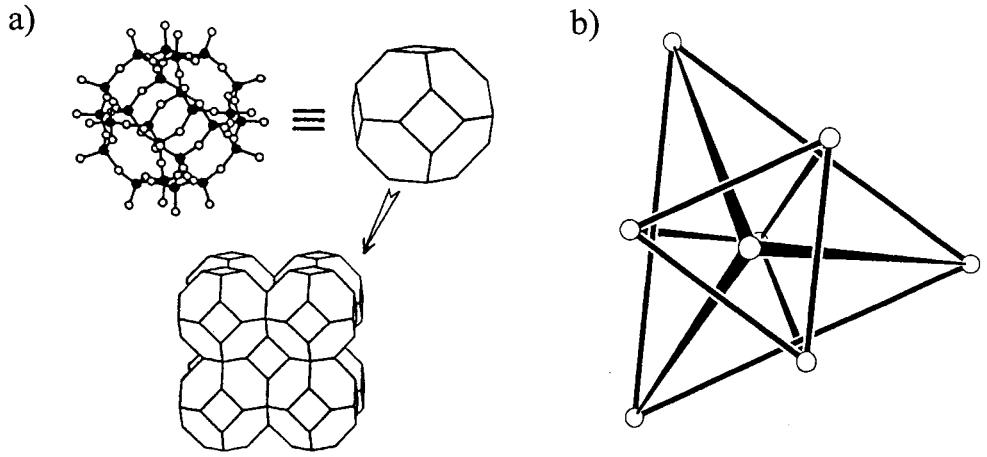

Figure 1. (a) Cage structure of the sodalite lattice. The filled and open circles in the upper left cage mark the Si^{IV} and Al^{III} and the oxygen ions, respectively. (b) Inner- and outer-sphere Na^+ coordination of the Cl^- ions, which center the β cages.

Lyot filter with a resolution of 0.1 nm (≅6 cm^{-1}). For the detection we applied the same setup as for the PL measurements. The PLE spectra were taken by tuning the laser wavelength, thereby recording the change of the sample luminescence at a fixed wavelength. The PLE technique was used instead of absorption spectroscopy because of the much better resolution and signal-to-noise ratio. Unfortunately, we were not able to extend the PLE measurements to energies above 18 000 cm^{-1}.

The powder reflectance measurements were performed with an "Ulbricht-sphere" under the conditions of diffuse reflection in the spectral range from 200 to 850 nm (12000−50000 cm^{-1}) at room temperature.

Polarized Raman spectra were recorded by a DILOR-XY spectrometer with a nitrogen cooled CCD camera as the detector (see ref 14 for details).

To compare the optical properties of the selenium sodalite with those of diselenium radicals in alkali metal halides, we prepared selenium-doped KI crystals applying the method of Vannotti et al.[18] The recorded spectra of the latter single crystals in comparison to those reported in the literature demonstrate the excellent signal-to-noise ratio and spectral resolution of the used experimental setup.

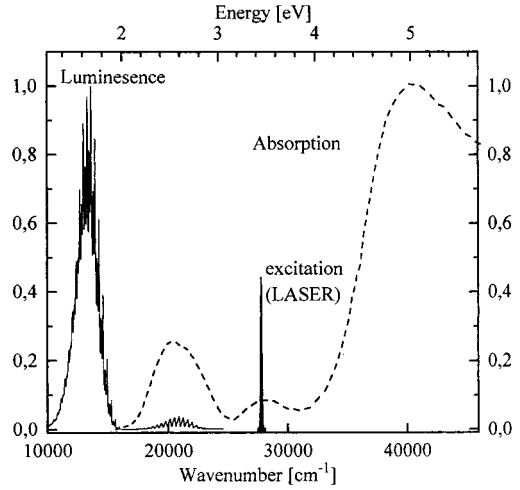

Figure 2. Diffuse reflectance (dashed curve) and—on a linear scale—luminescence spectrum (solid curve) of selenium-doped sodalite (intensity scale in arbitrary units).

3. Structural and Analytical Properties

Sodalite is a cubic zeolite-type compound of the space group $P\bar{4}3n$ (no. 219) with the composition $Na_8[Al_6Si_6O_{24}]Cl_2$. The sodalite cages are formed by corner-connected AlO_4 and SiO_4 tetrahedra (Figure 1a). The lattice constant of ≅8.8 Å corresponds to the dimension of one of the constituting β cages. Each cage is occupied by a regular $ClNa_4^{3+}$ tetrahedron with the point symmetry $\bar{4}$ (S_4) and a Cl^-−Na^+ spacing of 2.73 Å. Four additional Na^+ ions from neighboring cages at a distance of 4.96 Å constitute a second cationic coordination sphere, as illustrated in Figure 1b.

The structural refinement of the pink hydrothermally grown single crystals by X-ray diffraction yielded a composition very near that of a pure sodalite, the selenium content being below the limit of detection by X-rays. Microprobe investigations showed, however, that every 800th cage is occupied by a Se_2^- center. Powder samples of the red selenium ultramarine, prepared without addition of chloride, had the approximate composition $Na_7[Al_6Si_6O_{24}]Se_2$, indicating that only every second cage is occupied by Se_2^-.[4,5] The additionally appearing Na^+ deficiency gives evidence that not only Na_4^{4+} but also Na_3^{3+} polyhedra occur in the β cages. The presumable reason for these anionic and cationic deficiencies is the spacious Se_2^- anion, whose electron clouds may be estimated to extend over a distance of more that 4.5 Å in the bond direction—a value corresponding to twice the internuclear spacing of 2.25 Å. However, the available space for the anionic species in the Na_4^{4+} tetrahedra is only about 3.6 Å, which is the diameter of the Cl^- anion.[19] With these stereochemical arguments in mind it seems reasonable to assume that one Se_2^- center tends to replace one Cl^- ion and one Na^+ ion, to match with the host site dimensions, and leaving one neighboring Na_4^{4+} tetrahedron unoccupied for charge balance reasons. A trigonal-planar Na_3^{3+} coordination with an orientation of the Se_2^- radical along the C_3 axis will certainly reduce the sterical constraints. The discussed sterical mismatch also explains why single crystals can be grown only with very small percentages of Se_2^- radicals. The incorporation of larger amounts of the color center necessarily leads to pseudocrystalline powder materials, due to the steric strains and constraints just mentioned. Similar observations are made for the "lapislazuli", the blue sulfur ultramarine, where predominantly spacious S_3^- radical anions are the color centers.[17]

4. Results

4.1. Absorption and Raman Spectra. The powder reflectance spectrum of the red selenium ultramarine—which is identical with the single-crystal spectrum of the selenium-doped compound—is shown in Figure 2 as a dashed curve, together

(18) Vannotti, L.; Morton, J. *J. Chem. Phys.* **1967**, *47*, 4210.

(19) Shannon, R. D. *Acta Crystallogr.* **1976**, *A32*, 751.

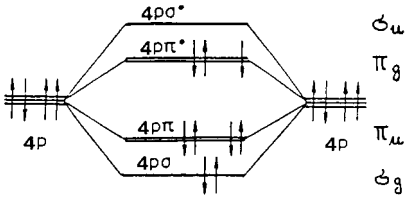

Figure 3. Molecular orbital scheme of Se_2^- radicals. The electron occupation approximately represents the $^2\Pi_g$ ground state. The excited $^2\Pi_u$ and $^2\Sigma_u^-$, $^2\Delta_u$ terms of Se_2^- correspond in crude approximation to the excitation of one electron from π_u into π_g and from π_u into σ_u, respectively. In the case of Se_2 with one electron less in the π_g MO ($\approx^3\Sigma_g^-$ ground state) the observed absorption and luminescence band involves the transition of one electron between π_u and π_g ($^3\Sigma_u^-$). See ref 21 for details.

with the luminescence of the pink single crystals (solid line). Three absorption bands are observed, from which the one with the highest intensity at 40 000 cm^{-1} is presumably correlated with an absorption process, which involves the release of an electron from Se_2^- into the sodalite frame (see below). The origin of the band cannot be traced back to the frame itself, because undoped zeolites absorb only above 50 000 cm^{-1}.[20] The two weaker bands—in the visible region at 20 000 cm^{-1} and in the UV range at 28 000 cm^{-1}—are due to transitions of diselenium species. The absorption at 20 000 cm^{-1} is assigned to the transition from the $^2\Pi_g$ ground state to the excited $^2\Pi_u$ term of Se_2^-. This is in satisfactory agreement with quantum chemical calculations of ground- and excited-state potential energy curves for the Se_2^- entity,[21] according to which this band possesses the highest intensity of all low-lying dipole- and spin-allowed transitions and should occur at 18 600 cm^{-1}. Under the band envelope the presence of the less intense transitions $^2\Pi_g \rightarrow {}^2\Sigma_u^-$ (19 650 cm^{-1}) and $\rightarrow {}^2\Delta_u$ (20 850 cm^{-1}) can be suspected.[21] The cited calculations also prove that the band at 28 000 cm^{-1}—which was proposed by Murata et al.[11] to be the $^2\Pi_g \rightarrow {}^2\Delta_u$ transition—cannot be caused by the Se_2^- color center. This argument is supported by the observation that—in contrast to the selenium sodalite—this transition is not always observed in the spectrum of Se_2^- in KI, its appearance somewhat depending on the synthesis procedure. We will come back to this point in section 4.3. The one-electron molecular orbital scheme in Figure 3 illustrates in an approximate description the nature of the above-mentioned electronic transitions.

In Figure 4 the Raman spectrum of a selenium-doped sodalite single crystal is depicted in comparison with that of bare sodalite. The latter consists of a few weak lines and one strong line at 464 cm^{-1}. The strong additional peaks are due to the chromophore Se_2^-, indicating a stretching frequency in the $^2\Pi_g$ ground state of 331 cm^{-1}—in good agreement with results published before[6] and a calculated value of 310 cm^{-1}.[21] Their intensities do not show a polarization dependence, indicating a statistical orientation of the Se_2^- dumbbells with respect to the axes of the cubic host structure—as expected.

4.2. Luminescence Spectrum. The 5 K luminescence spectrum of selenium-doped sodalite (Figure 5), using a logarithmic intensity scale so that also the low-intensity features of the spectrum can be distinctly seen, consists of two broad features. The one at 14 000 cm^{-1} is referred to as the "red" luminescence band and the second, considerably weaker one at 21 000 cm^{-1} as the "blue" luminescence band. It should be noted

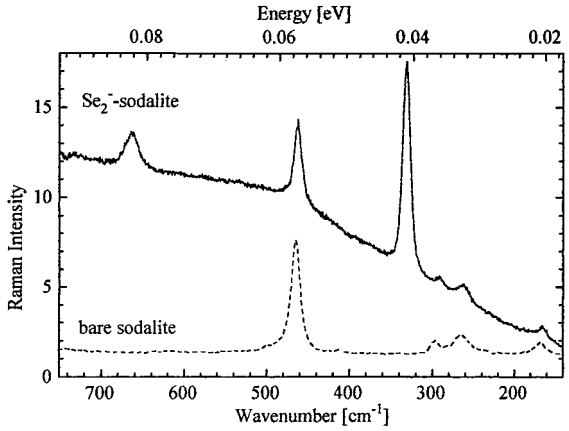

Figure 4. Raman spectrum of selenium-doped sodalite single crystals (solid line) and of bare sodalite (powder) for 514 nm (19 450 cm^{-1}) excitation.

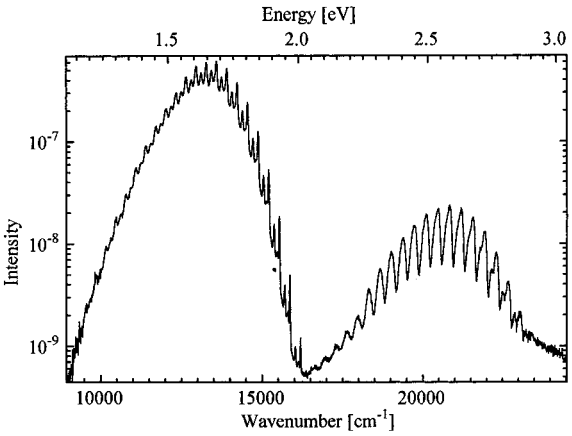

Figure 5. Emission spectrum of selenium-doped sodalite on the logarithmic intensity scale (excitation wavelength 364 nm, 27 470 cm^{-1}).

that the latter is only observed at the highest applied laser excitation energy of 27 470 cm^{-1}—which will be commented on below. Each band has a characteristic fine structure. The shape of the luminescence spectrum is different from that of selenium-doped alkali metal halides.[12] The latter do not emit in the region of the blue band, and the red luminescence is shifted to higher wavelengths compared to that of the selenium sodalite. Furthermore, the latter emission exhibits a different fine structure.

4.2.1. Red Luminescence. The emission of the pink selenium ultramarine single crystals at 14 000 cm^{-1} is depicted in Figure 6a, together with the corresponding excitation spectrum (PLE). As can be particularly deduced from the closeup in Figure 7b, a fine structure with alternating higher and lower intensity peaks is nicely resolved in both types of spectra, which will be labeled A and B in the following. Their intensity ratio is constant, depending neither on the sample temperature nor on the intensity of the exciting radiation, for example. Both the emission band at 14 000 cm^{-1} and the absorption band at 20 000 cm^{-1} correlate with the $^2\Pi_g \leftrightarrow {}^2\Pi_u$ transition, the energy difference of about 6000 cm^{-1} between them (Stokes shift) indicating a rather different intermolecular Se−Se spacing in the ground and excited states. For this transition a distinct polarization is expected in the $D_{\infty h}$ point group of the Se_2^- radical, with vanishing intensity perpendicular to the Se−Se bond direction. The selection rule would also hold when one Se_2^- dumbbell is placed in a sodalite cage such that the orientation matches either with one of the S_4 axes of a Na_4^{4+} tetrahedron or with the C_3

(20) Seifert, R.; Kunzmann, A.; Calzaferri, G. *Angew. Chem., Int. Ed.* **1998**, *37*, 1522.
(21) Heinemann, C.; Koch, W.; Lindner, G.-G.; Reinen, D.; Widmark, P.-O. *Phys. Rev. A* **1996**, *54*, 1979.

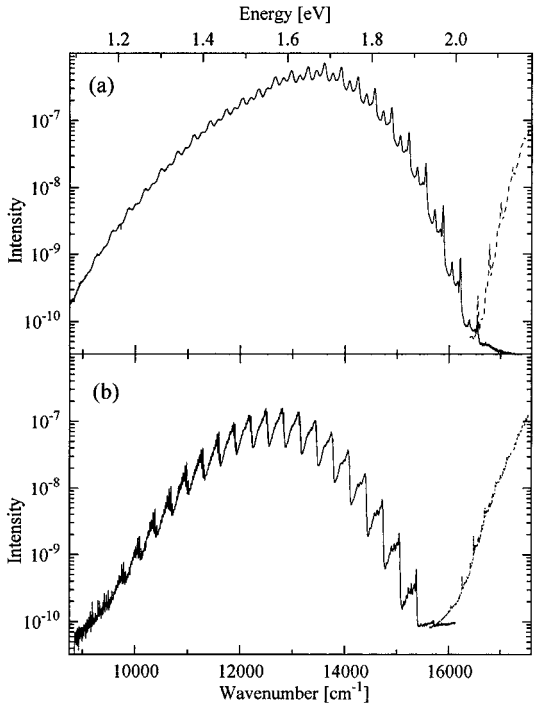

Figure 6. (a) Red luminescence (PL) band of selenium-doped sodalite (solid line), together with the luminescence excitation (PLE) spectrum (dashed line), excitation wavelength 514 nm (19 450 cm^{-1}), $T < 10$ K. (b) Luminescence spectrum of Se_2^- in KI (solid line), together with the PLE spectrum (dotted line), on the same scale and with the same measuring conditions as (a).

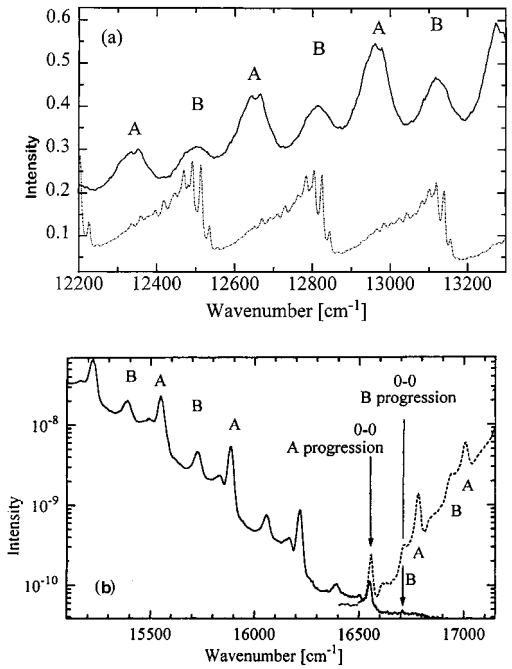

Figure 7. (a) Closeup of the red luminescence band in the region of maximum intensity, showing the well-resolved zero-phonon lines of the different selenium isotopes for Se_2^- in KI (dashed−dotted line), but only weak indications of the isotopic splitting for the sodalite host (solid line). The zero-phonon lines of the A and B progressions are marked in the latter case. (b) Closeup of Figure 6a, illustrating the crossing regions of the PL (solid line) and PLE (dashed line) spectra of Se_2^- in sodalite. The 0−0 transitions and the zero-phonon lines of the A and B progressions are marked.

axis of a cation-deficient Na_3^{3+} polyhedron. Because a polarization is observed neither in the red luminescence nor in the Raman spectrum, the Se_2^- color centers are statistically oriented with respect to the 3- and 4-fold axes at the cage center, as expected for a cubic lattice.

In Figure 6b the PL and PLE spectra of selenium-doped KI single crystals are shown for comparison, recorded under the same measuring conditions as those in Figure 6a. They are equivalent to those reported.[7−10] The fine structure is well understood, stemming from progressions of zero-phonon lines of the various selenium isotopes and of multiphonon side bands.[8,12,13]

A closeup of Figure 6 in the region of the maximum of the red emission bands is depicted in Figure 7a. While the isotope splitting is nicely resolved for Se_2^--doped KI, it is only indicated in the case of the selenium sodalite (A peaks). Apparently the chromophore is not sterically entirely fixed in the sodalite cages, and inhomogeneous broadening occurs. Comparing the fine structure of the red luminescence band for selenium-doped sodalite and KI, we deduce (see below) that the zero-phonon lines in both the A and B progressions have—within the error limit—the same energetic distance as in the KI case. In accord with the Raman data, the energy (334 cm^{-1}) is that of the Se_2^- stretching vibration in the $^2\Pi_g$ ground state.

To gain information on the physical origin of the A and B progressions, the corresponding spectroscopic constants of the zero-phonon lines are evaluated. In eq 1[22] $\bar{\nu}$ is the wavenumber

$$\bar{\nu} = \bar{\nu}_{00} - \varpi_0''\upsilon'' + \varpi_0''\chi_0''\upsilon''^2 \qquad (1)$$

of a zero-phonon line, corresponding to the transition from the vibrational level with quantum number $\upsilon' = 0$ in the excited state to a vibrational level with quantum υ'' in the ground state. The 0−0 transition $\bar{\nu}_{00}$ is the wavenumber difference between the levels with $\upsilon' = 0$ and $\upsilon'' = 0$. The fundamental vibrational energy ϖ_0'' and the anharmonicity parameter $\varpi''\chi_0''$ are the spectroscopic constants of the ground state. To calculate those, we need the energies of the 0−0 transitions.

The PL and PLE spectra of Se_2^--doped sodalite are shown as closeups in the crossing region in Figure 7b. The progressions of A and B types are seen in the PLE band as well and accordingly labeled. As an additional feature one observes a progression with broad and weak peaks, which are neighbors to the A lines in the PL and also in the PLE spectrum, with identical energetic distances to A in both cases. Therefore, we assign these peaks as multiphonon side bands of the A zero-phonon lines. The corresponding side bands to the B progression seem to be superimposed by the tails of the A lines and are hence not resolved. The low intensity of the multiphonon side bands gives further indication that the coupling of the color centers to the lattice phonons is weak.

The high resolution of the PL and PLE sodalite spectra allows the 0−0 transitions to be read directly (Figure 7b) and the quantum numbers υ' and υ'' to be assigned to the observed zero-phonon lines. The calculations of the spectroscopic constants were performed by a least-squares fit of the data to eq 1. The results given in Table 1 show that the spectroscopic constants ϖ_0'' and $\varpi_0''\chi_0''$ of the $^2\Pi_g$ ground state are almost the same for the A and B zero-phonon lines, and hence indicate that the shape and structure of the corresponding potential curves should be identical within the error limits. Unfortunately in the PLE spectrum a sufficiently large number of zero-phonon lines for the determination of the anharmonicity constant $\varpi_0''\chi_0''$ of the excited $^2\Pi_u$ potential curve is not observed.

(22) Herzberg, G. *Spectra of Diatomic Molecules*, 2nd ed.; Van Nostrand: Princeton, NJ, 1950.

Table 1. Spectroscopic Constants for the Ground State and First Excited State of Se_2^- in the Sodalite, as Well as for the Ground State of Intermediate Se_2 Diradicals in the Same Host[a]

state	series	$\bar{\nu}_{00}$ (cm^{-1})	ϖ_0'', ϖ_0' (cm^{-1})	$\varpi_0''\chi_0''$, $\varpi_0'\chi_0'$ (cm^{-1})	r_e (Å)	v'', v'
$^2\Pi_g$ (Se_2^-)	A	16 546	334	0.89	2.25	0−18
	B	16 719	334	0.83	2.25	0−18
$^2\Pi_u$ (Se_2^-)	A	16 547	224		2.56	0−4
	B	16 717	230		2.54	0−3
$^3\Sigma_g^-$ (Se_2)		23 816	386	1.2	2.17	0−20

[a] The calculated values of the internuclear distance r_e and the numbers of observed zero-phonon lines are also given.

Table 2. Se_2^--Doped KI: Spectroscopic Constants for the Ground State and the First Excited State of Se_2^-, Considering the Two Se Isotopes with the Greatest Abundance[a]

state	$\bar{\nu}_{00}$ (cm^{-1})	ϖ_0'', ϖ_0' (cm^{-1})	$\varpi_0''\chi_0''$, $\varpi_0'\chi_0'$ (cm^{-1})	r_e (Å)
$^2\Pi_g$ ($^{77}Se_2^-$)[b]	16 038	335	0.90	2.25
$^2\Pi_g$ ($^{80}Se_2^-$)[b]	16 037	329	0.86	2.25
$^2\Pi_u$ ($^{77}Se_2^-$)[c]	16 040	224	0.77	2.61
$^2\Pi_u$ ($^{80}Se_2^-$)[c]	16 040	216	0.62	2.61
$^3\Sigma_g^-$ ($^{80}Se_2$)[d]	23 874	385	0.96	2.17

[a] The calculated internuclear spacings in the various states are also given. [b,c] Data from own measurements, equivalent to those in refs 8 and 10, respectively. [d] The data for the Se_2 molecule in the $^3\Sigma_g^-$ ground state refer to that center in an argon matrix.[11]

In Table 2 the spectroscopic constants of Se_2^--doped KI are listed for the two selenium isotopes with the highest abundance. They agree with the values reported in the literature.[7,8,23] Comparing the results with those of Se_2^- in sodalite, one has to bear in mind that only mean values—averaged over the isotope splitting—are available in this case. Apparently the spectroscopic constants for the $^2\Pi_g$ ground-state potential curve only very slightly differ for the KI and sodalite host. The spectroscopic data collected in Tables 1 and 2 for the $^2\Pi_g$ and $^2\Pi_u$ states of Se_2^- in the sodalite and alkali metal halide matrices agree reasonably well with those which are deduced from quantum-mechanical calculations for the free radical anion.[21]

Afterall, the origin of the two progressions observed in the PL and PLE spectrum of the selenium-doped sodalite is still unclear. In alkaline metal halides as hosts different progressions of zero-phonon lines are also observed.[9] They are attributed to splittings of the doubly degenerate $^2\Pi_g$ ground and $^2\Pi_u$ excited states, caused by the orientation of the Se_2^- radical parallel to a C_2 axis of the octahedral cationic coordination, inducing a D_{2h} point symmetry.[9,10] For a splitting of this kind the intensity of the PL spectrum is expected to depend on the excitation energy and the intensity of the PLE spectrum on the detection wavelength.[8−10] Such observations are not made in the case of the sodalite host, and no temperature dependence of the intensity distribution between the A and B progressions is observed either. Thus, we conclude that the A and B progressions are due to two different chromophores, which we propose to be Se_2^- radicals in a trigonal Na_3^{3+} coordination and a tetrahedral Na_4^{4+} coordination, respectively. Both geometries do not induce a splitting, if the orientations of the Se_2^- entities are such that they correlate with the highest symmetry axes of those polyhedra—as has been discussed above. These orientations are also most favorable for geometric reasons, because here the chromophore volume matches the available space in an optimum way, avoiding steric constraints as much as possible.

From Figures 6 and 7 and Tables 1 and 2 we deduce that the red luminescence band of Se_2^- in sodalite is shifted to higher energies with respect to the corresponding band of Se_2^--doped KI, this blue shift being larger for the B chromophore than for the A chromophore. From the respective 0−0 transitions we estimate $\Delta\bar{\nu}_{00}$ to be 510 cm^{-1} for the A species and 680 cm^{-1} for the B species. One reason might be that the crystal field of the surrounding positive charges imposed on the Se_2^- radical in the sodalite cage with a cationic Na_4^{4+} or Na_3^{3+} coordination is different from that in the KI host, where the color center is situated in an octahedron of K^+ ions. However, the finding of a ground-state potential surface, which is almost identical in both cases (see section 4.3), shows that crystal field effects of this kind are small. This is also in agreement with our supposition that the chromophore is only weakly bonded to the sodalite matrix—and apparently also to the cationic K_6^{6+} environment in KI. Thus, we think that the steric constraint due to the unfavorable size relation between the Se_2^- radical—having an extension along the bond axis of about 4.5 Å—and the available space is of presumably deciding influence. In the sodalite cage Se_2^- replaces a Cl^- ion with the rather small diameter of 3.6 Å, as has been outlined before (see section 3), while the substitution of the spacious I^- anion with a diameter of 4.4 Å[7] in the KI host by Se_2^- seems possible without significant confinement effects. In the excited $^2\Pi_u$ state geometrical constraints should be even more severe in the sodalite cage, considering that the Se_2^- radical is expected to expand its electron cloud from 4.5 to about 5.2 Å, as has been estimated by using Clarks' rule.[24] The expansion is caused by exciting an electron from the π-bonding π_u into the π-antibonding π_g molecular orbital (Figure 3), which drastically reduces the stretching frequency of the Se_2^- anion (Tables 1 and 2). The destabilizing effect due to the geometric confinement slightly raises the excited potential curve, enhancing the $\bar{\nu}_{00}$ ($^2\Pi_g \leftrightarrow {}^2\Pi_u$) transition energy for the sodalite compared to that for Se_2^- in the KI host structure. Because the Na_4^{4+} tetrahedron provides less space for the chromophore than the Na_3^{3+} polyhedron with a cation deficiency, the steric constraints are expected to be larger in the former case. Hence, we assign the A and B progressions to Se_2^- in the trigonal-planar and tetrahedral coordinations, respectively. This is in accord with the about 1 order in magnitude lower intensity of the B lines, indicating only a minor fraction of Se_2^- in the Na_4^{4+} position. The proposed concept is supported by the stretching frequencies and estimated internuclear distances of Se_2^- in Tables 1 and 2. They are nearly identical in the sodalite and KI host for the ground state, but differ in the excited $^2\Pi_u$ state. Due to the anticipated steric constraint the internuclear Se−Se spacing r_e is smaller and the stretching frequency larger than in the case of the sodalite host. Apparently slight changes of these two parameters in the expected direction seem to occur also, when the A and B centers are compared.

4.2.2. Blue Luminescence. When the color centers in the sodalite are excited with a laser energy corresponding to 27 400 cm^{-1}, a blue luminescence is observed in addition to the red emission (Figure 5). The progression with $\omega_0'' = 386$ cm^{-1} is much larger than that observed in the red band ($\omega_0'' = 334$ cm^{-1}), in excellent agreement with the stretching frequency of the Se_2 molecule.[25] An assignment to this species is confirmed by the observation of the first zero-phonon line at $\bar{\nu}_{00} = 23\,816$ cm^{-1}, very near the energy of this transition reported for Se_2 in

(23) Gmelin, A. *Handbuch Anorgische Chemie 2A, Selenium*, Springer: Berlin, Heidelberg, New York, 1980; p 57 ff and references therein.
(24) Clark, C. *Phys. Rev.* **1935**, *47*, 238.
(25) Ahmed, F.; Nixon, E. 34th Symposium on Molecular Spectroscopy; 1979.

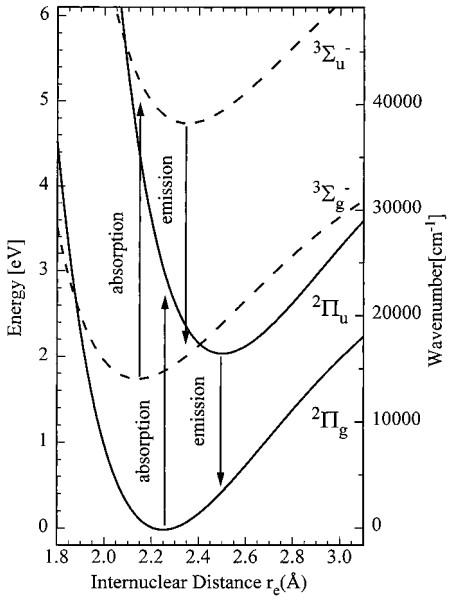

Figure 8. Schematic potential energy diagram of Se_2 (dashed lines) and Se_2^- (chromophore A, solid lines) in sodalite. The arrows mark the most intense optical transitions. The energy separation between the ground states of Se_2^- and Se_2 is obtained from the ionization energy of the Se_2^- anion. From the low-lying excited states only the one which is connected with the ground state by the largest dipole transition moment is shown for Se_2^- ($^2\Pi_u$) and Se_2 ($^3\Sigma_u^-$).

an argon matrix ($\bar{\nu}_{00}$ = 23 874 cm^{-1}).[26] The spectroscopic constants for the blue emission, which should correspond to the $^3\Sigma_u^- \rightarrow {}^3\Sigma_g^-$ transition (Figure 3) according to quantum-mechanical energy and intensity calculations,[21] are collected in Table 1, while Table 2 presents literature data. The internuclear distance of the Se_2 molecule in the excited state is 2.35 Å[27] and is hence expected to induce less severe confining effects than the excited Se_2^- radical.

When the color centers are excited with a wavelength of 514 nm (19 450 cm^{-1}), the red band of the Se_2^- chromophore appears in the luminescence spectrum exclusively. Using excitation energies, which lie in the range of the UV absorption band (28 000 cm^{-1}), however, the blue luminescence comes up in addition (Figure 5). Keeping in mind that the Raman spectrum shows only lines due to Se_2^- (Figure 4), we may hence readily conclude that the neutral Se_2 molecules are created photochemically during the UV laser excitation as intermediate species. This subject will be discussed further in the following section.

4.3. Potential Energy Curves of Se_2^- and Se_2 in Sodalite. The potential curves of the $^2\Pi_g$ and $^2\Pi_u$ terms of Se_2^- in sodalite (chromophore A) as well as that of the $^3\Sigma_g^-$ ground state of Se_2 in the same host were calculated by assuming a Morse-type potential[22] and by using the spectroscopic constants in Tables 1 and 2 (Figure 8). They are very similar to those derived from quantum-chemical calculations.[21] The potential curve of the first excited state $^3\Sigma_u^-$ of Se_2 was derived on the basis of the spectroscopic constants reported by Bondybye and English.[26] The minima of the excited $^2\Pi_u$ (Se_2^-*) and of the $^3\Sigma_g^-$ (Se_2) potential curves are placed such that the maximum intensity of the luminescence band occurs at the 10th (v_9'')—see Figures 6a and 7a—and 9th (v_8'')—Figure 5—zero-phonon lines, respectively. The energy difference between the ground states of Se_2 and Se_2^- is chosen according to the ionization energy of Se_2^- (14 500 cm^{-1}).[23]

The potential curves of the $^2\Pi_u$ and of the $^3\Sigma_g$- states cross, thus allowing one of the four π-antibonding electrons of the excited Se_2^-* radical ($\approx\sigma_g^2\pi_u^3\pi_g^4\sigma_u^0$) to gain energy by falling back into the π-bonding MOs, while a second one is ionized and transferred onto the sodalite lattice (see Figure 3). The latter electron is presumably stabilized by delocalization preferentially into Na_4^{4+} tetrahedra of unoccupied cages, neighboring to the cage, in which a Se_2 molecule is intermediately created (eq 2). Indeed, Na_4^{3+} clusters have been previously claimed to exist in zeolite-type structures.[28]

$$[Se_2^-Na_3]^{2+} \xrightarrow{h\nu} [Se_2^-*Na_3]^{2+}$$

$$[Se_2^-*Na_3]^{2+} + [Na_4]^{4+} \rightarrow [Se_2Na_3]^{3+} + [e^-Na_4]^{3+} \quad (2)$$

The generated Se_2 diradical may then be excited into the luminescing $^3\Sigma_u^-$ state by a second quantum of about 3.5 eV (vertical energy distance between the $^3\Sigma_g^-$ and $^3\Sigma_u^-$ potential curves in Figure 8). This energy matches the position of the UV absorption band in the optical spectrum (Figure 2) at 28 000 cm^{-1}. The excited Se_2* diradical relaxes into the $^3\Sigma_g^-$ ground state by the blue emission, subsequently transforming back into Se_2^-* ($^2\Pi_u$) by the uptake of the electron from the sodalite lattice and a corresponding electronic rearrangement. The possibility of the direct creation of Se_2* in the $^3\Sigma_g^-$ state in the luminescence experiment by the ionization of a Se_2^-** radical in a higher excited state than $^2\Pi_u$ (not shown in Figure 8) has to be rejected, because an excitation energy of about 5 eV is afforded for such a process—appreciably larger than the applied laser energy. The latter energy corresponds to that of the high-intensity UV band in the reflectance spectrum (Figure 2), however (see section 4.1).

Afterall the comparatively weak UV band at 28 000 cm^{-1} (Figure 2) very probably corresponds to the $^3\Sigma_g^- \rightarrow {}^3\Sigma_u^-$ transition of the Se_2 molecule, created under the energy conditions of the absorption measurement. This assignment might be proven by analyzing the zero-phonon line fine structure of the UV band. Unfortunately, single-crystal absorption spectra at low temperatures have not been recorded up to now.

5. Summary

The deeply colored ultramarine-type solids are simple model systems to investigate the optical properties of the Se_2^- and other chalcogen radicals in the cages of the sodalite structure.[17] The luminescence spectrum of selenium-doped sodalite single crystals consists of two bands, one in the red spectral region and the other in the blue spectral region, the former originating from the Se_2^- chromophore. The unique optical quality allowed the resolution of a remarkable fine structure in the red emission, consisting of two series of equally spaced zero-phonon lines. They presumably image Se_2^- color centers in two sites of different geometry. One possesses a tetrahedral coordination of four Na^+ cations, while the other is a position with a cation-deficient Na_3^{3+} coordination, which is preferentially present. Though the latter site is geometrically more flexible, both positions underlie significant steric constraints by the cationic environment, which are particularly efficient in the luminescing excited $^2\Pi_u$ state. The destabilizing effect of such confinement is nicely documented by a higher energy shift of the red luminesence with respect to the corresponding emission of Se_2^-

(26) Bondybey, V.; English, J. *J. Chem. Phys.* **1980**, *72*, 6479.
(27) Barrow, R.; Burton, W., Callomon, J. *Trans. Faraday Soc.* **1970**, *66*, 2685.
(28) Breuer, R.; Boer, E.; Geismar, G. *Zeolites* **1989**, *9*, 336.

in the more spacious KI host, which is larger for the chromophore in the Na_4^{4+} coordination than in the Na_3^{3+} coordination. The steric constraints also readily explain the tendency of Se_2^- to ionize, thus creating less voluminous Se_2 diradicals in the sodalite cages. The blue luminescence originates from the latter molecules, which are created and excited during UV irradiation in a process involving the ionization of the Se_2^- diradical into the extended frame of the sodalite structure. The simultaneous emission of Se_2^- color centers and intermediately generated Se_2 is here observed and reported for the first time. It is interesting to note in this connection that intermediate Te_2 radicals can be generated in tellurium-doped sodalites as well.[14] However, in contrast to the selenium case—depending on the preparation conditions—stable Te_2 species may appear in addition, which can be nicely identified by the Raman spectrum.

Acknowledgment. We are grateful to Dr. K. Witke of the Bundesanstalt für Material-Forschung und Prüfung, D-12480 Berlin, Germany, for measuring the Raman spectrum and discussions. Part of this work has been supported by the European Community ESPRIT III Basic Research Program, project SOLDES, and by the "Fonds der Chemischen Industrie".

IC990223U